Enhancing the Resolution of the Spectrogram of Non-Stationary Mobile Radio Channels by Using Massive MIMO Techniques

Matthias Pätzold
University of Agder
Faculty of Engineering and Science
NO-4898 Grimstad, Norway
Email: matthias.paetzold@uia.no

Carlos A. Gutierrez
Universidad Autonoma de San Luis
San Luis Potosi 78290, Mexico
Email: cagutierrez@ieee.org

***Abstract*—This paper is concerned with the enhancement of the resolution of the spectrogram of non-stationary mobile radio channels using massive multiple-input multiple-output (MIMO) techniques. By starting from a new generic geometrical model for a non-stationary MIMO channel, we derive the complex MIMO channel gains under the assumption that the mobile station (MS) moves with time-variant speed. Closed-form solutions are derived for the spectrogram of the complex MIMO channel gains by using a Gaussian window. It is shown that the window spread can be optimized subject to the MS's speed change. Furthermore, it is shown that the spectrogram can be split into an auto-term and a cross-term. The auto-term contains the useful time-variant spectral information, while the cross-term can be identified as a sum of spectral interference components, which restrict considerably the time-frequency resolution of the spectrogram. Moreover, it is shown that the effect of the cross-term can be drastically reduced by using massive MIMO techniques. The proposed method is not only important for estimating time-variant Doppler power spectra with high resolution, but it also pioneers the development of new passive acceleration/deceleration estimation methods and the development of new non-wearable fall detection systems.**

I. Introduction

The prospects that massive multiple-input multiple-output (MIMO) techniques will be a key component of 5G have boosted the research activities in the area of large-scale antenna systems. Over the past few years, the benefits of massive MIMO techniques have triggered studies on energy and spectral efficiency [1], [2], joint spatial division and multiplexing [3], channel estimation [4], performance evaluation [5], and 5G channel modelling [6].

In this paper, we propose another application of large-scale antenna systems aiming to enhance the spectral resolution of the spectrogram of non-stationary MIMO channels. A spectrogram is a mathematical tool that provides a time-frequency portrait of signals or stochastic processes. The spectrogram has been extensively used in speech analysis [7], classification of musical instruments [8], sonar detection of ships [9], radar [10], seismology [11], and remote sensing [12]. Applications of the spectrogram in the area of mobile radio channel modelling have first been introduced in [13], where the Doppler power spectral density of a multipath fading channel has been estimated by applying the concept of the spectrogram. The proposed procedure has recently been extended in [14] to the time-frequency analysis of single-input single-output (SISO) multipath fading channels under speed variations of the mobile station (MS). In [14], it was shown that the multipath components of the received signal cause spectral interferences, which limit the frequency resolution of the spectrogram considerably. The reduction of the spectral interference is a general problem in time-frequency signal analysis [15]. Although many attempts have been made to reduce the effects caused by spectral interferences (see., e.g., [16]–[21] and the references therein), none of the proposed methods have been completely successful. In this paper, we show how this problem can be solved by using massive MIMO techniques.

Our paper starts with the introduction of a new generic geometrical model for a MIMO channel in which the locations of the scatterers are not restricted to any particular geometry. From the proposed generic geometrical model, we derive the complex MIMO channel gains under the realistic assumption that the MS can change its speed. It turns out that the complex MIMO channel gains of all subchannels can be represented by a sum-of-chirps process, which does not fulfil the wide-sense stationary conditions. The spectrogram of the complex MIMO channel gain is derived in closed form and presented as a sum of an auto-term and a cross-term. While the auto-term reveals how the Doppler spectrum evolves over time, the cross-term restricts the resolution of the spectrogram by undesired spectral interference components. It is shown how massive MIMO techniques can be used to suppress the cross-term, which enhances the resolution of the spectrogram considerably.

The remainder of the paper is organized as follows. In Section II, the non-stationary MIMO channel model is derived by starting from a general geometrical model and taking into account that the velocity of the MS can change with time. Section III presents a closed-form solution of the spectrogram of the complex MIMO channel gains by using a Gaussian

DOI 10.1109/VTCFall.2017.8287886

window. The numerical results illustrating our main findings are presented in Section IV. Finally, the conclusion is provided in Section V.

II. Derivation of the Non-Stationary MIMO Channel Model

A. A Generic Geometrical Model

The starting point for the derivation of the non-stationary MIMO channel model is the generic geometric model shown in Fig. 1. This figure presents the downlink of a typical non-line-of-sight (NLOS) multipath propagation scenario in which the base station (BS) (transmitter) and the MS (receiver) are equipped with uniform linear antenna arrays consisting of M_T transmit and M_R receive antennas, respectively. The distance between the BS and the MS is denoted by D. In Fig. 1, the symbols δ_T (δ_R) and β_T (β_R) designate the antenna element spacing and the tilt angle of the transmitter (receiver) antenna array, respectively. The BS is supposed to be elevated and unobstructed by objects, while the MS is surrounded by N local scatterers S_n $(n = 1, 2, \ldots, N)$. The location of the nth scatterer S_n is determined by its distance r_n from the MS's origin as well as by the angle of arrival (AOA) α_n^R. Depending on the modelling assumptions, the distances r_n and AOAs α_n^R can be either random variables or constants or a combination of both. For example, if $r_n = R$ holds for all $n = 1, 2, \ldots, N$, where R is a constant, and if the AOAs α_n^R are independent and identically distributed (i.i.d.) random variables, each of which is uniformly distributed over $(0, 2\pi]$, then the geometrical model in Fig. 1 represents the well-known geometrical one-ring scattering model [22], [23], [24, Sect. 8.2.1] for an $M_T \times M_R$ MIMO channel in an isotropic propagation environment. Furthermore, it is assumed that the distance D is large compared to r_n, and that r_n in turn is large in comparison to the lengths of the antenna arrays, i.e., $D \gg r_n \gg \max\{(M_T - 1)\delta_T, (M_R - 1)\delta_R\}$ for all $n = 1, 2, \ldots, N$. As indicated in Fig. 1, the MS moves with a time-variant velocity $\vec{\mathrm{v}}(t)$ in a given direction determined by a fixed angle of motion (AOM) α_v. This implies that the speed $\mathrm{v}(t) = |\vec{\mathrm{v}}(t)|$ changes with time during the observation interval. Finally, we suppose that the distance which the MS moves during the observation interval is sufficiently small such that the AOAs α_n^R can approximately be considered as time invariant.

B. Modelling the Time-Variant Doppler Frequencies

In kinematics, *acceleration* and *deceleration* are two of the most important terms. The main difference between these terms is that acceleration refers to the rate of change of velocity, which can be either positive or negative, while deceleration refers to a negative rate of change of velocity. It is also known from kinematics that the velocity $\vec{\mathrm{v}}(t) = \mathrm{v}(t)\exp\{j\alpha_\mathrm{v}(t)\}$ is a vector, where its magnitude $|\vec{\mathrm{v}}(t)| = \mathrm{v}(t)$ is called speed, and $\alpha_\mathrm{v}(t)$ represents the AOM. In general, acceleration can be caused by a change in speed $\mathrm{v}(t)$ and/or a change in the AOM $\alpha_\mathrm{v}(t)$.

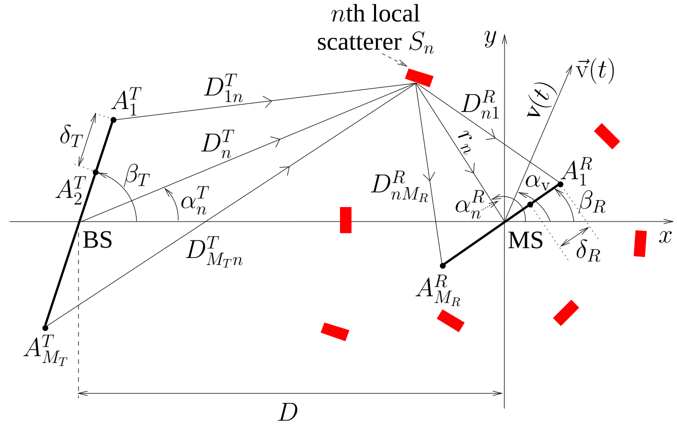

Fig. 1. Generic geometrical model for a non-stationary $M_T \times M_R$ MIMO channel with local scatterers S_n located irregularly around an MS (receiver) which moves with time-variant velocity $\vec{\mathrm{v}}(t)$.

In the following, we assume that the AOM is constant during the observation period of the channel, i.e., $\alpha_\mathrm{v}(t) = \alpha_\mathrm{v}$, and that the speed changes with a constant rate, denoted by a_0. For ease of terminology, we call a_0 acceleration if $a_0 > 0$ and deceleration if $a_0 < 0$, although strictly speaking acceleration can imply both $a_0 > 0$ and $a_0 < 0$. For constant values of a_0, it is obvious that the speed $\mathrm{v}(t)$ changes with time according to

$$\mathrm{v}(t) = \mathrm{v}_0 + a_0 t \tag{1}$$

where v_0 denotes the initial speed at $t = 0$, i.e., $\mathrm{v}_0 = \mathrm{v}(0)$. As a consequence of the time-variant speed $\mathrm{v}(t)$, the maximum Doppler frequency $f_{\max}(t)$ changes also with time according to the relation

$$f_{\max}(t) = \frac{f_0}{c_0}\mathrm{v}(t) = \frac{f_0}{c_0}(\mathrm{v}_0 + a_0 t) \tag{2}$$

where the symbols f_0 and c_0 are denoting the carrier frequency and the speed of light, respectively. By using (2), the instantaneous Doppler frequency $f_n(t)$ of the nth path, defined as $f_n(t) = f_{\max}(t)\cos(\alpha_n^R - \alpha_\mathrm{v})$, can be expressed as [25]

$$f_n(t) \quad = \quad f_n + k_n t \tag{3}$$

where

$$f_n \quad = \quad \frac{f_0}{c_0}\,\mathrm{v}_0 \cos(\alpha_n^R - \alpha_\mathrm{v}) \tag{4}$$

$$k_n \quad = \quad \frac{f_0}{c_0}\,a_0 \cos(\alpha_n^R - \alpha_\mathrm{v})\,. \tag{5}$$

By invoking the phase-frequency relationship [15, Eq. (1.3.40)]

$$f_n(t) = \frac{1}{2\pi}\frac{d\theta_n(t)}{dt} \tag{6}$$

it has been shown in [25] that the instantaneous phase $\theta_n(t)$ of the nth path can be presented in the following form

$$\theta_n(t) = \theta_n + 2\pi\left(f_n t + \frac{k_n}{2}t^2\right) \tag{7}$$

where the initial phases $\theta_n = \theta_n(0)$ are modelled by i.i.d. random variables, each of which is characterized by a uniform distribution over the interval from 0 to 2π, i.e., $\theta_n \sim \mathcal{U}(0, 2\pi]$.

C. Modelling of the Complex MIMO Channel Gains

Let $h_{k\ell}(t)$ denote the complex channel gain of a narrowband $M_T \times M_R$ MIMO channel describing the link from the ℓth transmitter antenna A_ℓ^T ($\ell = 1, 2, \ldots, M_T$) to the kth receiver antenna A_k^R ($k = 1, 2, \ldots, M_R$). By starting from the geometrical model in Fig. 1 and applying the design steps of the generalized principle of deterministic channel modelling [24, Sect. 8.1], it can be shown that the complex MIMO channel gains $h_{k\ell}(t)$ can be expressed as (without proof)

$$h_{k\ell}(t) = \sum_{n=1}^{N} g_{k\ell n}\, e^{\,j\left[2\pi\left(f_n t + \frac{k_n}{2} t^2\right) + \theta_n\right]} \tag{8}$$

for $k = 1, 2, \ldots, M_R$ and $\ell = 1, 2, \ldots, M_T$, where

$$g_{k\ell n} = a_{\ell n}\, b_{kn}\, c_n\, d_n \tag{9}$$

$$a_{\ell n} = e^{\,j\pi(M_T - 2\ell + 1)\frac{\delta_T}{\lambda_0}\left[\cos(\beta_T) + \frac{r_n}{D}\sin(\beta_T)\sin(\alpha_n^R)\right]} \tag{10}$$

$$b_{kn} = e^{\,j\pi(M_R - 2k + 1)\frac{\delta_R}{\lambda_0}\cos\left(\alpha_n^R - \beta_R\right)} \tag{11}$$

$$d_n = e^{-j\frac{2\pi}{\lambda_0}\left\{D + r_n\left[1 + \cos(\alpha_n^R)\right]\right\}} \tag{12}$$

and c_n denotes the path gain of the nth path. Depending on the design objectives, each of the model parameters $c_n, \alpha_n^R, \theta_n$, and r_n can be a random variable or a constant. If at least one of these model parameters is a random variable and N is infinite (finite), then $h_{k\ell}(t)$ in (8) represents a stochastic reference (simulation) model for a non-stationary MIMO channel. On the other hand, if all model parameters $c_n, \alpha_n^R, \theta_n$, and r_n are constant and N is finite, then $h_{k\ell}(t)$ describes a deterministic simulation model. For the computation of the path gains c_n and AOA α_n^R (or alternatively, the initial Doppler frequencies f_n), a variety of parameter computation methods have been developed (see, e.g., [24, Sect. 5.4]). The phases θ_n are usually assumed to be either i.i.d. random variables with uniform distribution or outcomes (realizations) of uniformly distributed random variables, which implies that the phases θ_n are constants in such cases. Finally, the distances r_n can be computed in accordance with any given delay profile by using the procedure presented in [26].

The non-stationary MIMO channel model described by (8) includes a variety of other channel models as special cases. For example, if the acceleration a_0 is zero and if all the scatterers S_n are located on a ring of radius R, i.e., $r_n = R$ for $n = 1, 2, \ldots, N$, then the non-stationary complex channel gain $h_{k\ell}(t)$ in (8) reduces to the wide-sense stationary complex channel gain of the well-known one-ring model [22], [23], [24, Sect. 8.2.2]. Furthermore, for the special case of a single-input single-output (SISO) channel, where $M_T = M_R = 1$ holds, it follows that the phase terms $a_{\ell n}$ [see (10)] and b_{kn} [see (11)] are equal to 1, and thus the complex channel gain $h_{k\ell}(t)$ in (8) reduces to that of the non-stationary SISO channel model introduced in [25].

In a nutshell, we can say that if an MS increases or decreases its speed linearly with time, then the complex channel gain $h_{k\ell}(t)$ of an $M_T \times M_R$ MIMO channel can be modelled by a sum of chirps, as presented in (8). From the expression in (8), it is important to realize that the instantaneous Doppler frequencies $f_n(t) = f_n + k_n t$ of $h_{k\ell}(t)$ are the same for all sub-channels, i.e., for all $k = 1, 2, \ldots, M_R$ and $\ell = 1, 2, \ldots, M_T$. For random phases θ_n and fixed values of c_n, f_n, and k_n, we would intuitively expect that the Doppler power spectral density of $h_{k\ell}(t)$ is time variant and given by

$$S_{h_{k\ell}}(f, t) = \sum_{n=1}^{N} c_n^2\, \delta(f - f_n - k_n t)\,, \tag{13}$$

where $\delta(\cdot)$ denotes the Dirac delta function. In the next section, we will show how the time-variant spectral characteristics of $h_{k\ell}(t)$ can be estimated by using the concept of the spectrogram.

III. Spectrogram of the Non-Stationary MIMO Channel Model

A. Review of the Spectrogram

The basic idea of the spectrogram is to break a time-varying signal up into overlapping short-time signals. The spectrogram is then defined as the squared magnitude of the Fourier transform of the overlapping short-time signals. The concept of the spectrogram is widely used for gaining insight into how the spectral characteristics of a signal or stochastic process vary over time.

The short-time signal $x_{k\ell}(t', t)$ of the complex MIMO channel gain $h_{k\ell}(t)$ is obtained by multiplying $h_{k\ell}(t)$ by a window functions $w(t)$ centred at t, i.e.,

$$x_{k\ell}(t', t) = h_{k\ell}(t)w(t' - t) \tag{14}$$

where t' denotes the running time, and t represents the observation time being a fixed point in time at which we are interested in the local spectral characteristics of $h_{k\ell}(t)$. An example for a short time signal is shown in Fig. 2 for the case of a Gaussian window function

$$w(t) = \frac{1}{\sqrt{\sqrt{\pi}\sigma_w}}\, e^{-\frac{t^2}{2\sigma_w^2}} \tag{15}$$

where σ_w denotes a real-valued constant called the *window spread parameter*. It should be noted that the window function $w(t)$ is even and positive and has unit energy, i.e., $\int_{-\infty}^{\infty} w^2(t)\, dt = 1$. The short-time Fourier transform (STFT) $X_{k\ell}(f, t)$ of the complex MIMO channel gain $h_{k\ell}(t)$ is defined as the Fourier transform of the short-time signal $x_{k\ell}(t', t)$ with respect to the running time t', i.e.,

$$X_{k\ell}(f, t) = \int_{-\infty}^{\infty} x_{k\ell}(t', t)\, e^{-j2\pi f t'} dt'\,. \tag{16}$$

Finally, from the STFT $X_{k\ell}(f, t)$, the spectrogram $S_{h_{k\ell}}(f, t)$ of $h_{k\ell}(t)$ is obtained as

$$S_{h_{k\ell}}(f, t) = |X_{k\ell}(f, t)|^2\,. \tag{17}$$

The time resolution and frequency resolution of the spectral components of $S_{h_{k\ell}}(f,t)$ depend on the window spreading parameter σ_w. A larger value of σ_w enhances the resolution in frequency, but worsens the resolution in time and vice versa. An optimum solution to this trade-off problem is presented in the next subsection.

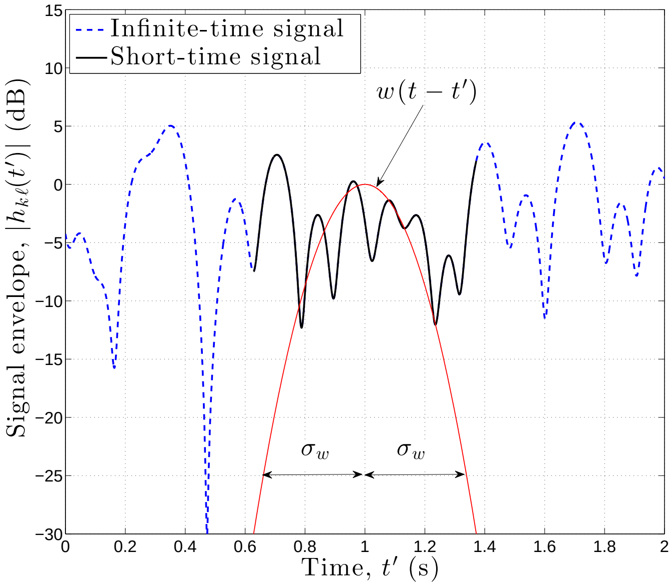

Fig. 2. Example of a fading signal $h_{k\ell}(t)$, which is supposed to be unlimited in time, and the corresponding short-time signal $x_{k\ell}(t',t)$ obtained by using a Gaussian window $w(t)$ with window spread parameter σ_w.

B. Derivation of the Spectrogram

Substituting the complex MIMO channel gain $h_{k\ell}(t)$ [see (8)] and the Gaussian window function $w(t)$ according to (15) in (14) and computing the Fourier transformation of $x_{k\ell}(t',t)$ with respect to t' according to (16) results after several mathematical manipulations in the following closed-form solution of the STFT (without proof)

$$X_{k\ell}(f,t) = \frac{e^{-j2\pi f t}}{\sqrt{\sqrt{\pi}\sigma_w}} \sum_{n=1}^{N} G(f, f_n(t), \sigma_x^2)\, h_{k\ell n}(t) \qquad (18)$$

where

$$G\left(f, f_n(t), \sigma_x^2\right) = \frac{1}{\sqrt{2\pi}\sigma_x} e^{-\frac{(f-f_n(t))^2}{2\sigma_x^2}} \qquad (19)$$

$$\sigma_x^2 = \frac{1 - j2\pi\sigma_w^2 k_n}{(2\pi\sigma_w)^2} \qquad (20)$$

$$h_{k\ell n}(t) = g_{k\ell n}\, e^{j\left[2\pi\left(f_n t + \frac{k_n}{2} t^2\right) + \theta_n\right]}. \qquad (21)$$

In the equations above, $f_n(t), f_n, k_n$, and $g_{k\ell n}$ are given by (3), (4), (5), and (9), respectively. After substituting the STFT $X_{k\ell}(f,t)$ according to (18) in (17) and performing some mathematical manipulations, we obtain the following closed-form solution of the spectrogram (without proof)

$$S_{h_{k\ell}}(f,t) = S_{h_{k\ell}}^{(a)}(f,t) + S_{h_{k\ell}}^{(c)}(f,t) \qquad (22)$$

where

$$S_{h_{k\ell}}^{(a)}(f,t) = \sum_{n=1}^{N} c_n^2\, G\left(f, f_n(t), \sigma_n^2\right) \qquad (23)$$

$$S_{h_{k\ell}}^{(c)}(f,t) = \frac{2}{\sqrt{\pi}\sigma_w} \sum_{n=1}^{N-1} \sum_{\substack{m=2 \\ m>n}}^{N} \mathrm{Re}\left\{G\left(f, f_n(t), \sigma_x^2\right) G^*(f, f_m(t), \sigma_x^2)\, h_{k\ell n}(t)\, h_{k\ell m}^*(t)\right\} \qquad (24)$$

and

$$\sigma_n^2 = \frac{1 + (2\pi\sigma_w^2 k_n)^2}{2(2\pi\sigma_w)^2}. \qquad (25)$$

The first term in (22) is called the *auto-term*, while the second term is said to be the *cross-term*.

The auto-term $S_{h_{k\ell}}^{(a)}(f,t)$ contains the desired spectral information. The result in (23) states that the auto-term $S_{h_{k\ell}}^{(a)}(f,t)$ equals a sum of Gaussian functions, each of which is weighted by the squared path gain c_n^2 and centred at the corresponding instantaneous Doppler frequency $f_n(t)$. The spread of the instantaneous Doppler frequency $f_n(t)$ is determined by the variance σ_n^2 in (25). In the limit $\sigma_n^2 \rightarrow 0$, the Gaussian function $G(f, f_n(t), \sigma_n^2)$ tends to the Dirac delta function $\delta(f - f_n(t))$, and thus the auto-term $S_{h_{k\ell}}^{(a)}(f,t)$ of the spectrogram approaches to the intuitively expected time-variant Doppler power spectrum $S_{h_{k\ell}}(f,t)$ in (13). Unfortunately, the variance σ_n^2 cannot be set to zero, as σ_n^2 is a function of the window spread parameter σ_w and the quantity k_n [see (25)]. However, the variance σ_n^2 can be minimized by computing $d\sigma_n^2/d\sigma_w^2$ and setting the result to zero. This results in the following optimum value of the window spread parameter

$$\sigma_{w,\mathrm{opt}} = \frac{1}{\sqrt{2\pi|k_n|}} \qquad (26)$$

which in turn leads to the smallest possible value of the spread of $f_n(t)$

$$\sigma_{n,\min} = \sqrt{\frac{|k_n|}{2\pi}}. \qquad (27)$$

An interesting observation is that the product of $\sigma_{w,\mathrm{opt}}$ and $\sigma_{n,\min}$ is constant, namely $\sigma_{w,\mathrm{opt}}\sigma_{n,\min} = 1/(2\pi)$. This equation states that a larger window spread results in a smaller spread of the nth spectral component around the instantaneous Doppler frequency $f_n(t)$.

The cross-term $S_{h_{k\ell}}^{(c)}(f,t)$ in (24) can be interpreted as an undesired interference term consisting of $N(N-1)/2$ components. From (24), it is obvious that the cross-term $S_{h_{k\ell}}^{(c)}(f,t)$ is real-valued but not necessarily a positive function. Especially the latter property prevents the interpretation of $S_{h_{k\ell}}^{(c)}(f,t)$ as a power spectral density. In the next subsection, we will introduce two methods for reducing the cross-term $S_{h_{k\ell}}^{(c)}(f,t)$.

C. Methods for Reducing the Cross-Term of the Spectrogram

1) Reducing the Cross-Term by Phase Averaging: By comparing (23) with (24), we notice that the auto-term $S^{(a)}_{h_{k\ell}}(f,t)$ is independent of the phases θ_n, whereas the cross-term $S^{(c)}_{h_{k\ell}}(f,t)$ depends on θ_n. In fact, if the phases θ_n are i.i.d. random variables with uniform distribution $(0, 2\pi]$, then the cross-term $S^{(c)}_{h_{k\ell}}(f,t)$ can be removed completely from the spectrogram $S_{h_{k\ell}}(f,t)$ by averaging over θ_n, i.e.,

$$\begin{aligned} E\left\{S_{h_{k\ell}}(f,t)\right\}\big|_{\theta_n} &= E\left\{S^{(a)}_{h_{k\ell}}(f,t)\right\}\Big|_{\theta_n} + E\left\{S^{(c)}_{h_{k\ell}}(f,t)\right\}\Big|_{\theta_n} \\ &= S^{(a)}_{h_{k\ell}}(f,t) \\ &= \sum_{n=1}^{N} c_n^2\, G\left(f, f_n(t), \sigma_n^2\right) \end{aligned} \tag{28}$$

where $E\{\}$ denotes the expected value operator. Note that in (28), we have used the properties $E\{S^{(a)}_{h_{k\ell}}(f,t)\} = S^{(a)}_{h_{k\ell}}(f,t)$ and $E\{S^{(c)}_{h_{k\ell}}(f,t)\} = 0$.

This method is obviously very effective in laboratory experiments, where multiple fading signals $h_{k\ell}(t)$ can be generated by means of computer simulations using the same key parameters influencing (8) but different realizations (outcomes) of the phases θ_n.

2) Reducing the Cross-Term by Using Massive MIMO Techniques: The second method uses massive MIMO techniques to reduce the spectral interference caused by the cross-term $S^{(c)}_{h_{k\ell}}(f,t)$. This method is motivated by the fact that two different complex MIMO channel gains $h_{k\ell}(t)$ and $h_{k'\ell'}(t)$ have the same auto-term but different cross-terms if $k \neq k'$ and/or $l \neq l'$. This follows from the antenna steering factors $a_{\ell n}$ and b_{kn} in (10) and (11), respectively, which have different phases for different values of $\ell = 1, 2, \ldots, M_T$ and $k = 1, 2, \ldots, M_R$. Hence, the basic idea of the second cross-term reduction method is to compute the average of the cross-term $S^{(c)}_{h_{k\ell}}(f,t)$ in the spatial domain. Let $\bar{S}^{(c)}_{h_{k\ell}}(f,t)$ denote the (spatial) sample mean of the cross-term, defined by

$$\bar{S}^{(c)}_{h_{k\ell}}(f,t) = \frac{1}{M_R M_T}\sum_{k=1}^{M_R}\sum_{\ell=1}^{M_T} S^{(c)}_{h_{k\ell}}(f,t) \tag{29}$$

then a quantitative measure of the effectiveness of this method is the area under the absolute value of $\bar{S}^{(c)}_{h_{k\ell}}(f,t)$, i.e.,

$$P_X^{(c)} = \int_0^{T_{\text{obs}}}\int_{-\infty}^{\infty} \left|\bar{S}^{(c)}_{h_{k\ell}}(f,t)\right| df\, dt \tag{30}$$

which is called the *cross-power*, where T_{obs} denotes the observation interval. It is obvious that the spatial averaging does not affect the auto-term $S^{(a)}_{h_{k\ell}}(f,t)$, as (23) reveals that $S^{(a)}_{h_{k\ell}}(f,t)$ is independent of the number of transmit and receive antennas.

The second proposed method is of great advantage for the estimation of the spectral characteristics of measured mobile radio channels under non-stationary conditions if only single and not reproducible snapshot measurements of the complex channel gains $h_{k\ell}(t)$ are available. This is in general the case when channel measurements are taken under real-world propagation conditions.

IV. Numerical Results

This section presents some selected numerical results to visualize the key results of our findings. We consider a car braking scenario, in which the driver suddenly applies the brake to avoid an accident that could happen if a child suddenly runs into the street or a cyclist runs a stop sign. To simulate such a scenario, we set the initial speed v_0 to $\mathrm{v}_0 = 30\,\text{km/h}$ and the speed deceleration parameter a_0 to $a_0 = -4.166\,\text{m/s}^2$. In the considered propagation scenario, we have set the number of multipath components N to 10. The extended method of exact Doppler spread (EMEDS) [27] has been used to compute the path gains c_n and AOAs α_n^R according to

$$c_n = \sigma_0\sqrt{\frac{2}{N}}, \quad \alpha_n^R = \frac{2\pi}{N}\left(n - \frac{1}{4}\right) + \alpha_{\mathrm{v}} \tag{31}$$

with parameter $\sigma_0 = 1$ and AOM $\alpha_{\mathrm{v}} = 0°$. The phases θ_n have been considered as constant quantities obtained from the outcomes of a random generator with uniform distribution over $(0, 2\pi]$. The carrier frequency f_0 was chosen to be 5.9 GHz, which corresponds to a wavelength of $\lambda_0 = 5.0812\,\text{cm}$ and results in an initial maximum Doppler frequency of $f_{\max_0} = f_{\max}(0) = 164\,\text{Hz}$. The antenna element spacings were set to $\delta_T = \delta_R = \lambda_0/2$, and the antenna tilt angles were equal to $\beta_T = \beta_R = \pi/2$. The distance D between the transmitter and the receiver was supposed to be 500 m. Regarding the distribution of the scatterers S_n, we have assumed that they are located on a ring of radius $R = 50\,\text{m}$, i.e., $r_n = R = 50\,\text{m}$ for $n = 1, 2, \ldots, N$. For the window spread parameter σ_w, we have chosen the optimum value that follows from $\sigma_{w,\text{opt}} = 1/\sqrt{2\pi|k_1|}$. Finally, we choose an observation interval T_{obs} of 2 s during which the speed of the car slows down from 30 km/h to 0 km/h.

Fig. 3 shows the spectrogram $S_{h_{k\ell}}(f,t)$ of the complex channel gain $h_{k\ell}(t)$ for a 2×2 MIMO channel described by (8) for $k = \ell = 1$. This figure visualizes that the spectral components approach rapidly to zero during the full brake application lasting two seconds. The corresponding auto-term $S^{(a)}_{h_{k\ell}}(f,t)$ and cross-term $S^{(c)}_{h_{k\ell}}(f,t)$ are depicted in Figs. 4 and 5, respectively. As can be seen in Fig. 3, the two largest and smallest spectral components cannot be resolved. The limited resolution of the spectrogram $S_{h_{k\ell}}(f,t)$ is due to the strong interference components of the cross-term $S^{(c)}_{h_{k\ell}}(f,t)$ presented in Fig. 5. A perfect removal of the cross-term $S^{(c)}_{h_{k\ell}}(f,t)$ would result in the auto-term $S^{(a)}_{h_{k\ell}}(f,t)$ which resolves the two largest (smallest) instantaneous Doppler frequencies $f_n(t)$, as can be seen in Fig. 4. A significant reduction of the spectral interferences caused by the cross-term $S^{(c)}_{h_{k\ell}}(f,t)$ can be achieved by spatial averaging using massive MIMO techniques. This statement is supported by the results shown in Fig. 6, which renders the cross-power $P_X^{(c)}$ as a function of the number of transmit and receive antennas for MISO, SIMO, and MIMO systems with $M_T = M_R = M$. The behaviour of the cross-power $P_X^{(c)}$ clearly shows that the resolution of the spectrogram of non-stationary mobile radio channels can be enhanced considerably by using massive MIMO techniques.

V. Conclusion

In this paper, we have analysed the spectrogram of non-stationary MIMO mobile radio channels. Starting from a generic geometrical model for a MIMO channel with irregularly distributed local scatterers around the MS, we have derived a new non-stationary model for the complex MIMO channel gains under the realistic assumption that the MS can change its speed. It has been shown that the spectrogram of the complex MIMO channel gain can be separated into two parts comprising an auto-term, which contains an desired time-variant spectral information, and an undesired cross-term. For both terms, closed-form solutions have been presented. One of our key results was that the influence of the cross-term can drastically be reduced by using massive MIMO techniques.

The proposed method will enable a wide range of new applications, ranging from enhanced spectral estimation techniques for non-stationary mobile radio channels over passive acceleration/deceleration estimation methods for collision avoidance to the development of new non-wearable fall detection systems.

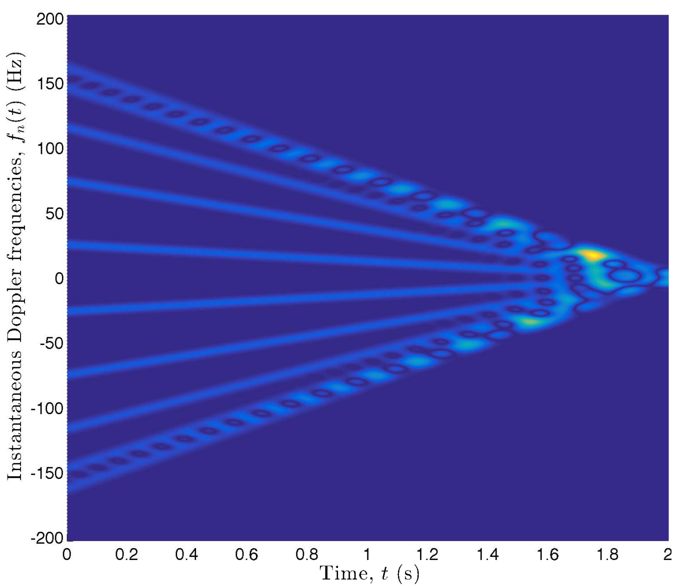

Fig. 3. Spectrogram $S_{h_{k\ell}}(f,t)$ of the complex channel gain $h_{k\ell}(t)$ designed by using the EMEDS with $N = 10$ for $k = \ell = 1$.

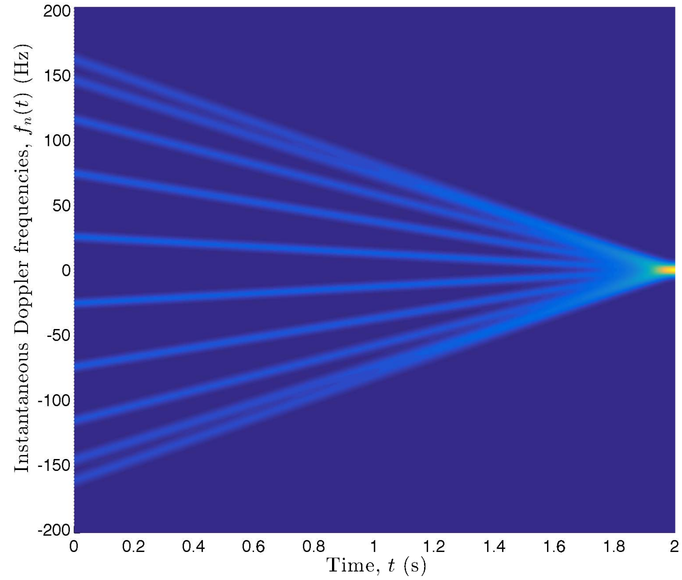

Fig. 4. Auto-term $S^{(a)}_{h_{k\ell}}(f,t)$ of the spectrogram $S_{h_{k\ell}}(f,t)$ of the complex channel gain $h_{k\ell}(t)$ designed by using the EMEDS with $N = 10$ for $k = \ell = 1$.

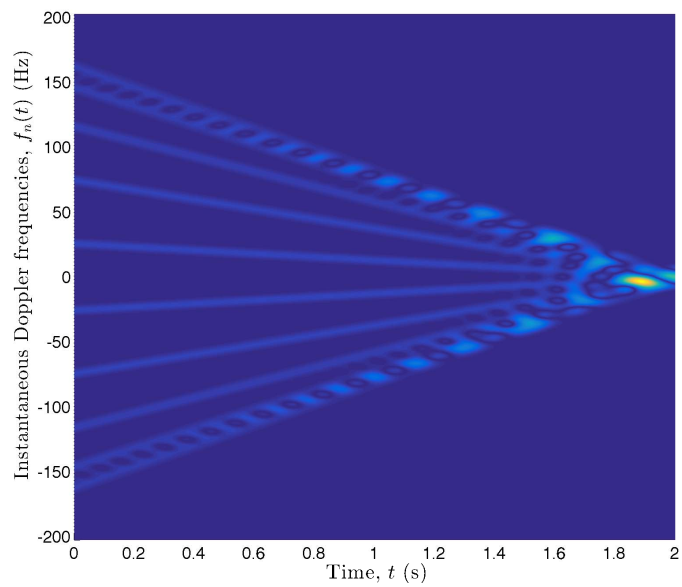

Fig. 5. Cross-term $S^{(c)}_{h_{k\ell}}(f,t)$ of the spectrogram $S_{h_{k\ell}}(f,t)$ of the complex channel gain $h_{k\ell}(t)$ designed by using the EMEDS with $N = 10$ for $k = \ell = 1$.

References

[1] H. Q. Ngo, E. G. Larsson, and T. L. Marzetta, "Energy and spectral efficiency of very large multiuser MIMO systems," *IEEE Trans. Commun.*, vol. 61, no. 4, pp. 1436–1449, Apr. 2013.

[2] E. Björnson, E. G. Larsson, and T. L. Marzetta, "Massive MIMO for maximal spectral efficiency: How many users and pilots should be allocated?" *IEEE Trans. Wireless Commun.*, vol. 15, no. 2, pp. 1293–1308, Feb. 2016.

[3] A. Adhikary *et al.*, "Joint spatial division and multiplexing for mm-wave channels," *IEEE J. Select. Areas Commun.*, vol. 32, no. 6, pp. 1239–1255, Jun. 2014.

[4] H. Yin, D. Gesbert, M. Filippou, and Y. Liu, "A coordinated approach to channel estimation in large-scale multiple-antenna systems," *IEEE J. Select. Areas Commun.*, vol. 31, no. 2, pp. 264–273, Feb. 2013.

[5] X. Gao, O. Edfors, F. Rusek, and F. Tufvesson, "Massive MIMO performance evaluation based on measured propagation data," *IEEE Trans. Wireless Commun.*, vol. 14, no. 7, pp. 3899–3911, Jul. 2015.

[6] S. Hur *et al.*, "Proposal on millimeter-wave channel modeling for 5G cellular system," *IEEE Trans. Signal Processing*, vol. 10, no. 3, pp. 454–469, Apr. 2016.

[7] J. R. Deller, Jr., J. H. L. Hansen, and J. G. Proakis, *Discrete-Time*

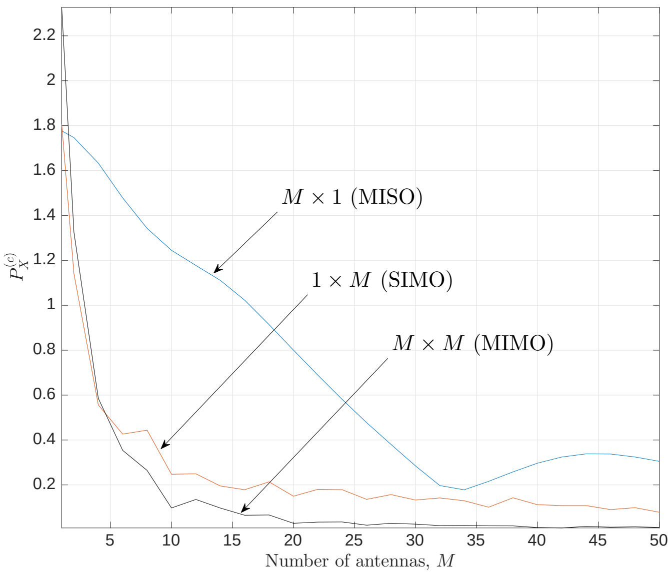

Fig. 6. Behaviour of the cross-power $P_X^{(c)}$ in terms of the number of transmit and receive antennas for MISO, SIMO, and MIMO systems, where $M_T = M_R = M$.

Processing of Speech Signals. Wiley-IEEE Press, 1999.

[8] J. F. Alm and J. S. Walker, "Time-frequency analysis of musical instruments," *SIAM Review*, vol. 44, no. 3, pp. 457–476, 2002.

[9] J. G. Lourens, "Passive sonar detection of ships with spectrograms," in *Proc. South African Symp. on Commun. Sign. Processing, COMSIG 1990*, Jun. 1990, pp. 147–151.

[10] R. I. A. Harmanny, J. J. M. de Wit, and G. Prémel Cabic, "Radar micro-Doppler feature extraction using the spectrogram and the cepstrogram," in *Proc. 11th European Radar Conference, EuRAD 2014*, Oct. 2014, pp. 165–168.

[11] C. I. Huerta-Lopez, Y. J. Shin, E. J. Powers, and J. M. Roesset, "Time-frequency analysis of earthquake records," in *Proc. 12th World Conf. on Earthquake Engineering, 12WCEE2000*, vol. 33. Auckland, New Zealand, Feb. 2000, pp. 1–9.

[12] T. A. Lampert and S. E. M. O'Keefe, "A survey of spectrogram track detection algorithms," *Applied Acoustics*, vol. 71, no. 2, pp. 87–100, Feb. 2010.

[13] M. Pätzold and N. Youssef, "Spectrogram analysis of multipath fading channels," in *Proc. 26th IEEE Personal, Indoor and Mobile Radio Communications, PIMRC 2015*. Hong Kong, China, Aug./Sep. 2015.

[14] M. Pätzold and C. A. Gutiérrez, "Spectrogram analysis of multipath fading channels under variations of the mobile speed," in *Proc. 84rd IEEE Veh. Technol. Conf., IEEE VTC2016-Fall*. Montreal, Canada, Sep. 2016.

[15] B. Boashash, Ed., *Time-Frequency Signal Analysis and Processing: A Comprehensive Reference*, 2nd ed. Elsevier Academic Press, 2015.

[16] J. Ville, "Théorie et applications de la notion de signal analytique," *Cables et Transmissions*, vol. 2A, no. 1, pp. 61–74, 1958, In French. English translation: I. Selin, *Theory and applications of the notion of complex signal*, Rand Corporation Report T-92 (Santa Monica, CA, Aug. 1958).

[17] D. Gabor, "Theory of communication," *J. IEE*, vol. 93[III], pp. 429–457, Nov. 1946.

[18] C. H. Page, "Instantaneous power spectra," *J. of Applied Physics*, vol. 23, no. 8, pp. 103–106, Jan. 1952.

[19] A. W. Rihaczek, "Signal energy distribution in time and frequency," *IEEE Trans. Inform. Theory*, vol. 14, no. 3, pp. 369–374, May 1968.

[20] M. J. Levin, "Instantaneous spectra and ambiguity functions (Corresp.)," *IEEE Trans. Inform. Theory*, vol. 10, pp. 95–97, Jan. 1964.

[21] L. Cohen, "Time-frequency distributions–A review," *Proceedings of the IEEE*, vol. 77, no. 7, pp. 941–981, Jul. 1989.

[22] D.-S. Shiu, G. J. Foschini, M. J. Gans, and J. M. Kahn, "Fading correlation and its effect on the capacity of multielement antenna systems," *IEEE Trans. Commun.*, vol. 48, no. 3, pp. 502–513, Mar. 2000.

[23] A. Abdi, J. A. Barger, and M. Kaveh, "A parametric model for the distribution of the angle of arrival and the associated correlation function and power spectrum at the mobile station," *IEEE Trans. Veh. Technol.*, vol. 51, no. 3, pp. 425–434, May 2002.

[24] M. Pätzold, *Mobile Radio Channels*, 2nd ed. Chichester: John Wiley & Sons, 2011.

[25] M. Pätzold and C. A. Gutiérrez, "The Wigner distribution of sum-of-cisoids and sum-of-chirps processes for the modelling of stationary and non-stationary mobile channels," in *Proc. 83rd IEEE Veh. Technol. Conf., IEEE VTC2016-Spring*. Nanjing, China, May 2016.

[26] A. Borhani and M. Pätzold, "On the spatial configuration of scatterers for given delay-angle distributions," *IAENG Engineering Letters*, vol. 22, no. 1, pp. 34–38, 2014.

[27] M. Pätzold, B. O. Hogstad, and N. Youssef, "Modeling, analysis, and simulation of MIMO mobile-to-mobile fading channels," *IEEE Trans. Wireless Commun.*, vol. 7, no. 2, pp. 510–520, Feb. 2008.